**A Tiered Approach to Human Synapse Proteomics: Optimized LC-MS/MS Analysis of Whole-Tissue and Synaptosome Preparations from Frozen Post-Mortem Brain Samples**

Femke C. Roig-Kuhn[1], Remco V. Klaassen[1], Frank T.W. Koopmans[1], Tiara S.Z. Koolman[1], August B. Smit[1], Sabine Spijker[1,*]

[1] Dept. of Molecular and Cellular Neurobiology, Vrije Universiteit Amsterdam, De Boelelaan 1100, 1081 HV, Amsterdam, the Netherlands:

* Correspondence s.spijker@vu.nl

Recent advancements in neuroproteomics have enabled detailed analysis of protein expression and function in the human brain. Post-mortem human brain studies have significantly advanced our understanding of the relationship between genetics, cell biology of neurological and psychiatric disorders and their clinical diagnosis. Given the central role of the synapse in these disorders, we evaluated the sensitivity of liquid chromatography-tandem mass spectrometry (LC-MS/MS) to detect synaptic proteins in whole-tissue lysates versus synaptosome preparations. First, we optimized sample preparation protocols for frozen human gray matter (GM), refining the suspension TRAPping (S-TRAP) digestion method to improve protein solubilization using thin tissue sections and to accomplish low technical variation by minimizing sample handling. Together, we achieved a highly reproducible sample preparation workflow by rigorously applying standardization and randomization across dissection, processing, and LC-MS/MS runs. Comparative LC-MS/MS analysis showed that whole-tissue lysates are practical for large-scale studies and broadly detecting synaptic proteins. However, enrichment by synaptosome isolation offered improved resolution of synapse-specific proteins. Because synapse-proteomics enables insight into spatial regulation—i.e., alterations at the synapse that are not reflected in the soma– we recommend a tiered approach: initial whole-tissue analysis for broad disease-associated changes, followed by targeted synaptosome proteomics to deepen insight into synaptic alterations. This strategy optimally balances throughput, reproducibility, and biological relevance, and enhances the study of brain disorders through proteomics. Moreover, analyzing synaptic proteins first at the tissue level improves insight into overall regulation of synaptic proteins induced by synapse loss or gain.

**Keywords:** Shotgun neuroproteomics; Frozen tissue; Human; Synapse proteomics; ProtiFi S-TRAP

## Introduction

Molecular techniques to study neurodegenerative and neuropsychiatric disorders are becoming increasingly precise and comprehensive. With the advent of high-throughput omics analyses like transcriptomics and proteomics, it is now possible to characterize the molecular signatures that distinguish specific disorders from healthy controls in large patient cohorts. This aids tremendously in uncovering underlying disease mechanisms, as a prelude to researching new treatment options. Yet, quantitative analyses on large cohorts pose many questions on how to best prepare and analyze the samples in a manner tailored to the specific research project.

One of the most direct methods to investigate differences between health and disease in humans is using frozen post-mortem brain tissue, made available by brain banks globally, with the ultimate goal of increasing the understanding of the human brain [1]. In addition to limitations in the quantity of brain tissue available from brain banks, omics studies face several key challenges. Chief among these are issues related to tissue quality—particularly the post-mortem interval—which can lead to degradation of RNA and proteins. Sample heterogeneity, including differences in age, sex, cause of death, medication use, and comorbid conditions, further complicates data interpretation. Technical challenges in sample preparation, such as variability and batch effects, also pose significant obstacles. These factors are especially critical in research on neuropsychiatric disorders, which often lack clear neuropathological markers. Moreover, proteomic alterations in these conditions are typically subtle and highly variable, reflecting the inherent biological complexity of human brain tissue. Careful experimental design, rigorous methodological controls, and minimizing technical variation — particularly during protein extraction and mass spectrometry [2]— are therefore essential to obtain meaningful insights.

In addition, subcellular fractionation can be of added value when performing proteomic analyses. In the brain, adaptations in synaptic connections determine neural network physiology and can be affected under disease conditions. Synaptic alterations have previously been associated with neurodegenerative disorders [3,4] and neuropsychiatric disorders [5–7]. As such, synaptic fractionation is a great approach to study the disease-specific regulation at the synapse. By isolating the synaptic compartment, it is possible to investigate subtle changes in proteins specific to the synapse that would otherwise not be detected in the lysate due to dilution in the whole-tissue context. Moreover, synaptic fractionation reduces sample complexity, making it possible to detect more low-abundant synaptic proteins with mass spectrometry. However, it is important to evaluate the extent of enrichment of synaptic proteins in synaptic isolations over whole-tissue preparations. Previous research in mice has revealed that there are brain region specific differences in synaptic protein enrichment [8], but the extent to which these differences translate to human brain tissue is unclear.

To evaluate the sensitivity of liquid chromatography-tandem mass spectrometry (LC-MS/MS) to detect synaptic proteins in whole-tissue lysates versus synaptosome preparations, we first implemented a standardized and randomized workflow that reduces sample handling and batch effects. Limiting sample handling has the additional benefit of increasing the feasibility of large-scale studies with several hundreds of samples [9–11]. We adapted a revised version of the ProtiFi suspension-trapping (S-TRAP) mini spin column digestion protocol 4.1 (ProtiFi,

New York, USA) previously described by our lab [12], in which sequence of dissection, sample preparation, and LC-MS/MS analysis was carefully arranged and randomized to avoid confounding effects.

Here, we will describe 1) an optimized digestion protocol to maximize peptide and protein yield for LC-MS/MS using thin post-mortem sections as input material, and 2) a comparison between whole-tissue and synaptosome proteomics, exploring the added advantages of enriching for synapses given recent improvements in mass spectrometry sensitivity. By outlining the rationale behind each step, we aim to support researchers in designing and executing robust and reproducible quantitative proteomic analyses on post-mortem brain tissue.

## Materials and Methods

### *Tissue Collection from Human Brain Samples*

Tissue was obtained from the Netherlands Brain Bank (NBB). Informed consent was obtained from all donors for the use of material and clinical data for research purposes. The NBB autopsy procedures and the use of tissue for research were approved by the Ethics Committee of Amsterdam UMC, location VUmc, Amsterdam, The Netherlands.

For optimizing the proteomics workflow, we used tissue from the most anterior part of the superior frontal gyrus (SFG) –comprising sections 2-7, as presented in the Adult Human Allen Brain Reference Atlas [13], overlapping with the medial and lateral subdivision of Brodmann area 9 and 10– of two samples from a non-demented control donor (NDC) and two samples from a donor diagnosed with (presenile) Alzheimer's Disease (AD) and (putative) comorbid schizophrenia (Supplemental file 1). For analysis of whole-tissue lysates vs. synaptosome preparations, we used the same anterior tissue of the SFG of 8 NDC donors (Table 1). For all samples, gray matter (GM) was collected from tissue sections (2–5 mg cut at 10 µm for whole-tissue lysate; ~25 mg cut at 50 µm for synaptosome preparations) using a cryostat.

***Table 1.*** *Demographic and clinical information of the superior frontal gyrus samples used in subcellular fraction isolation (synaptosome proteomics). NA: not measured. Braak LB: Braak Lewy Bodies. PMI: post-mortem interval. APOE: apolipoprotein E allele.*

| NDC donors (n = 8) | |
|---|---|
| Female/male n | 4/4 |
| Age median (range) | 88 (83-93) |
| Braak median (range) | 2 (0-3) |
| Braak LB (n) | 0 (1), 2 (1), 3 (1), NA (5) |
| PMI median (range) | 06:48 (05:05-10:00) |
| pH median (range) | 6.67 (6.20-7.12) |
| APOE (n) | 3-3 (1), NA (7) |

### *Adaptation of the ProtiFi S-TRAP Mini Spin Column Digestion Protocol 4.1 for LC-MS/MS Proteomics Analysis*

Tissue (2–5 mg) was extracted by adding 500 µL 5% sodium dodecyl sulfate (SDS) extraction buffer to the tissue sample, followed by incubation at 95 °C for 15 minutes, then at 55 °C for

another 15 minutes, to reduce disulfide bonds and alkylate cysteine residues. For a detailed and step-by-step description, see Supplemental protocol 1. For protein quantification, 8% of each sample was set aside for S-TRAP preparation, and 1.5% was used for the bicinchoninic acid (BCA) protein assay analysis. The remaining sample was stored in aliquots at -80 °C for later use. For S-TRAP, samples were diluted in the extraction buffer based on the BCA protein assay results to obtain aliquots containing 10 µg of total protein, which were then transferred to plasmid DNA micro-spin columns for Trypsin / Lys-C digestion (37 °C overnight). The following day, peptides were eluted and lyophilized. After resuspension, one-fifth of each sample was used in duplicate for a peptide assay to quantify peptide concentration. Based on these measurements, 150 ng of peptide was loaded onto an activated Evotip (Evosep, Odense C, Denmark). After completing the wash steps, the Evotips were stored at 4 °C until LC-MS/MS analysis.

***Subcellular Fraction Isolation: Synaptosome Proteomics***

Cortical GM tissue (~25 mg, sectioned at 50 µm) was homogenized in a homogenization buffer. For a detailed and step-by-step description, see Supplemental protocol 2. The resulting homogenate was centrifuged, and supernatant was placed on a sucrose gradient. The samples were then subjected to ultracentrifugation for two hours. The interphase disk between sucrose concentrations, containing the synaptosome fraction, was collected. After centrifugation, the pellet was resuspended, and the samples were set aside for S-TRAP. The samples were analyzed with the same adaptation of the ProtiFi S-TRAP mini spin column digestion protocol as described in the previous section, the only difference being the protein extraction: 35 µL of each synaptosome sample were added to 35 µL of 2x extraction buffer containing 10% SDS. For these samples, a BCA protein assay was performed after extraction, and the amount of protein was calculated based on absorption values. Trypsin was added in a 1:25 ratio and the samples were incubated at 37 °C overnight. The samples then underwent the same protocol as previously described to measure the resulting peptides with mass spectrometry.

***Mass Spectrometry and Data Analysis***

Mass spectrometry was performed using an Evosep One LC using a 15 cm × 150 µm reverse-phase column packed with 1.5 µm C18-beads (EV1137 from Evosep, Denmark) connected to a 20 µm ID ZDV emitter (Bruker Daltonics, Germany). Peptides were electro-sprayed into a timsTOF Pro2 mass spectrometer (Bruker Daltonics, Germany) equipped with CaptiveSpray source and measured with the following settings: Scan range 100-1700 m/z, ion mobility 0.65 to 1.5 Vs/cm2, ramp time 100 ms, accumulation time 100 ms, and collision energy decreasing linearly with inverse ion mobility from 59 eV at 1.6 Vs/cm2 to 20 eV at 0.6 Vs/cm2. Operating in dia-PASEF mode, each cycle took 1.38 s and consisted of 1 MS1 fµLl scan and 12 dia-PASEF scans. Each dia-PASEF scan contained two dia-PASEF isolation windows, in total covering 300-1200 m/z and ion mobility 0.65 to 1.50 Vs/cm2. Dia-PASEF window placement was optimized using the py_diAID tool[14]. Ion mobility was auto calibrated at the start of each sample (calibrant m/z, 1/K0: 622.029, 0.992 Vs/cm2, 1008 922.010, 1.199 Vs/cm2, 1221.991,

1.393 Vs/cm2). Samples were processed in a randomized manner to prevent batch effects by MS run order (Supplemental Figure S1).

The dia-PASEF raw data were processed with DIA-NN (version 1.8.1; [15]) for database search and MS-DAP (version 1.2.1; [16]). An in-silico spectral library was generated from the Uniprot human reference proteome (SwissProt and TrEMBL, release 2023-02) using Trypsin/P digestion and at most 1 missed cleavage. Fixed modification was set to beta-methylthiolation(C) and variable modifications were oxidation(M) and N-term M excision (at most 1 per peptide). Precursor charge range was set to 2-4, precursor m/z range was limited to 280–1220, both MS1 and MS2 mass accuracy were set to 15 ppm, scan window was set to 10, double-pass mode and match-between-runs were enabled. RT-dependent cross-run normalization was enabled with the robust LC quantification strategy. Protein identifiers (isoforms) were used for protein inference. All other settings were left as default.

MS-DAP 1.0.5 [16] was used for downstream analysis. Peptide-level filtering was configured to retain only peptides that were confidently identified in at least 50% of the samples per group. Peptide abundance values were normalized using the VSN algorithm, followed by protein-level mode-between normalization. Differential expression analysis (DEA) was performed in a between-subject manner by the MSqRob algorithm and resulting P-values were adjusted for multiple testing using the Benjamini–Hochberg False Discovery Rate (FDR) procedure. Significantly different proteins were determined with adjusted P-value cutoff of 0.05. The effect size of a regulated protein represents the ratio of relative (log2) fold change to the mean abundance variance across biological replicates.

Downstream analysis differed between the optimization of the protocol (peptides identified in 50% of samples per group; ≥1 peptides per protein; FDR = 5%), and the lysate-synaptosome comparison (peptides identified in 75% of samples per group; ≥2 peptides per protein; FDR = 5%). Differential expression analysis was performed using MSqRob, accounting for relevant covariates (sex, age). The online tool SynGO was used for gene set enrichment analysis in the synapse [17], focusing on gene ontology terms for cellular components. ShinyGO (v0.82; [18]) was used to indicate overrepresentation of specific pathways for synaptome enriched or lysate enriched contrasts (in Figures 4, 5) with standard settings (FDR cutoff 5%) except for increasing the minimal pathway size from 2 to 3 proteins and showing the top 10 pathways instead of top 20 (in Figure 4). Venn diagrams were made with InteractiVenn [19].

## Results

In this study, we employed tissue sectioning to selectively collect GM from frozen brain samples. This method is relatively straightforward and allows for precise anatomical targeting. Moreover, the use of thin (10 µm) tissue sections results in a high surface area-to-volume ratio, which facilitates efficient chemical solubilization. We first optimized our pre-MS workflow using thin GM sections and subsequently applied this protocol to compare whole-tissue lysates with synaptosome-enriched preparations derived from the same donor cohort.

### *1. Adaptation of the ProtiFi S-TRAP Mini Spin Column Digestion Protocol 4.1 for LC-MS/MS Proteomics Analysis for sectioned post-mortem tissue*

To perform neuroproteomic analyses of fresh-frozen human GM cortical tissue using a one-tube workflow with minimal sample handling, we adapted the ProtiFi S-TRAP mini spin column digestion protocol (version 4.1) to our sample input type (human GM) and quantity (2–5 mg tissue sectioned at 10 µm). We performed a pilot study to optimize lysis temperature, SDS buffer volume, and trypsin digestion conditions to ensure optimal protein solubilization and digestion. Protein solubilization is critical for ensuring replicability of samples, as variations in input material largely impact experimental outcomes. This is specifically important in neurodegenerative research, where protein aggregates (e.g. plagues, tangle) are frequently observed and often constitute key pathological features for molecular analysis [20]. To account for these factors in our pilot study, we used protein samples derived from 10 mg tissue to avoid exceeding solubilization limits. Moreover, tissue was collected from an NDC and AD donor, anticipating that AD samples might present a higher degree of protein aggregation, potentially affecting solubilization efficiency.

We first tested qualitative aspects of the solubilization protocol, focusing on SDS buffer volume and solubilization temperature. We avoided adding extra physical solubilization steps to reduce sample handling and instead aimed at improving the chemical solubilization in SDS buffer by making the collected tissue sections thinner and increasing the surface area in contact with the buffer. We determined that a volume of 500 µL of buffer was optimal, as this was sufficient to solubilize all the tissue without reaching the 1.5 mL Eppendorf tube volume limit. Higher volumes led to tissue loss due to sample trapping inside the lid during vortexing, whereas lower volumes resulted in incomplete dissolution into the SDS buffer. The optimal temperature for solubilization was 95 °C for all sample types (NDC and AD). However, this caused an undesired pressure build-up during vortexing. To mitigate this, the temperature was set to 95 °C for 15 minutes, followed by 55 °C for another 15 minutes, maintaining the original 30-minute solubilization time. Additionally, securing the tube lids prevented accidental opening of the safe-lock lids due to temperature-induced pressure increase.

Next, we quantified protein yield from a 10 mg tissue sample to determine the maximum amount of protein for digestion and adjusted the amount of trypsin accordingly. A 10 mg tissue sample represented the maximum tissue weight acquired during tissue collection, with average samples ranging between 2–5 mg. BCA assays showed no substantial difference in protein content between NDC and AD samples (Supplemental Figure S2) with approximately 9% of the tissue weight corresponding to protein (± 0.9 mg protein per 10 mg GM tissue). Based on these findings, a fixed amount of 1 µg trypsin was used for all samples.

Subsequently, we tested the effectiveness of the 95 °C solubilization step during protein extraction compared to 55 °C in terms of protein yield, as measured quantitatively by MS analysis. We also assessed whether centrifugation following solubilization affected the number of peptides and proteins identified, as this step could remove larger insoluble aggregates, and make the sample more homogeneous. For these tests, we compared samples of the previous NDC and AD donors, which were centrifuged or not after solubilization at 55 °C or 95 °C. All samples were processed with an adaptation of the S-TRAP Protifi protocol (Supplemental protocol 1), run through mass spectrometry using an Evosep One LC coupled to a timsTOF Pro2 HT instrument. The raw MS data was processed with DIA-NN for

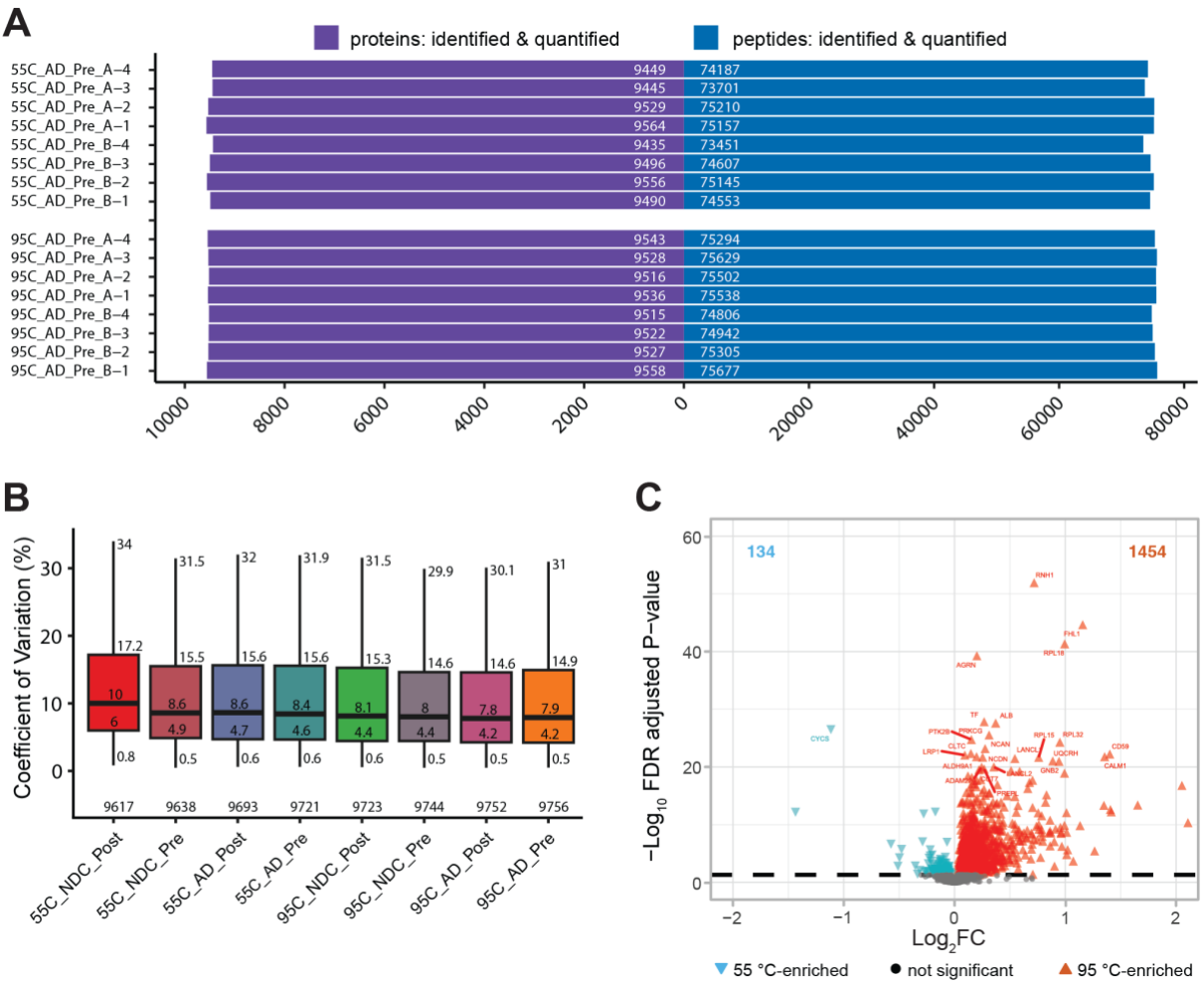


***Figure 1. Quality control parameters for one-tube tissue lysate protocol.*** *A) Comparison of protein and peptide levels between solubilization at 55 °C and 95 °C for the two AD donor samples was made from the pre-centrifugation samples. For a complete account of protein and peptide counts of all pilot experiments, see Supplemental Figure S3. In total, 4 replicates were taken per tissue sample. B) Protein-level coefficient of variation plots of all sample conditions. Values of quartiles and whiskers, and total number of proteins are indicated. A higher temperature during solubilization (95 °C) resulted in a small reduction of coefficient of variation. C) Volcano plot of MSqRob results showing the comparison of protein levels after solubilization at 55 °C vs. 95 °C in the 4 pooled replicates of the 2 NDC samples prior to centrifugation. Gene symbols are shown for the top 25 proteins with lowest FDR adjusted p-value. The total number of differentially expressed proteins (all above dashed black line) is indicated at the top (left, turquoise; right, red). Pre = pre-centrifugation; Post = post-centrifugation; NDC = non-demented control donor; AD = donor with Alzheimer's Disease and comorbid schizophrenia; A = donor A; B = donor B. For a complete list of proteins, see Supplemental file 1.*

database search and MS-DAP for downstream analysis (peptide detection rate 50%; ≥1 peptides per protein; FDR = 5%).

Solubilization at 95 °C yielded approximately the same protein and peptide counts compared to 55 °C in NDC, along with more consistent results in yield (Figure 1A). An added benefit of solubilization at 95 °C was the slight decrease in coefficient of variation, apparently reducing (technical) variability between samples (Figure 1B). Higher temperature solubilization led to

increased abundance levels (enriched at 95 °C) for a substantial portion of the detected proteins (1454/7444 = 19.53%), while only a small fraction showed decreased abundance levels (enriched at 55 °C; 134/7444 = 1.80%) (Figure 1C). Based on these findings, we selected 95 °C as the solubilization temperature for the subsequent synaptosome proteomics experiment (see section 2 & Supplemental protocol 1). The number of proteins not detected at all at 55 °C (189/(189+7444) = 2.48%) or 95 °C (160/(160+7444) = 2.10%) was very low, indicating that solubilization in this one-tube reaction was optimal, most likely due to the very thin tissue sections (10 µm) creating sufficient exposure to the chemical solubilization.

Subsequent centrifugation of the samples did not lead to substantial protein loss, regardless of solubilization temperature or sample type (NDC or AD) (Figure 2). At both 55 °C (Supplemental Figure S4) and 95 °C (Figure 2), the few proteins that were less abundant due to centrifugation included collagens (95 °C: NDC: 12/7502 proteins = 0.16%; AD: 10/7524 proteins = 0.13%), while some ribosomal proteins appeared paradoxically more abundant (95 °C: NDC: 6/7502 proteins = 0.08%; AD: 9/7524 proteins = 0.11%) (Figure 2). The proteins for which no peptides were detected –i.e., truly "lost" proteins after centrifugation– were only a small fraction of the total amount (95 °C: NDC: 61/(7502+61) = 0.81%; AD: 79/(7524+79) = 1.04%; Supplemental file 1). However, the fraction of proteins only detected after centrifugation (i.e., "lost" prior to centrifugation) were similar (95 °C: NDC: 66/(7502+66) = 0.87%; AD: 62/(7524+62) = 0.82%; Supplemental file 1), indicating that this mainly resulted from detection of proteins by chance levels of low abundant proteins. Since overall protein loss was minimal, we decided to retain the centrifugation step in the protocol. This step ensures a more representative sampling of the extracted proteins by removing potential

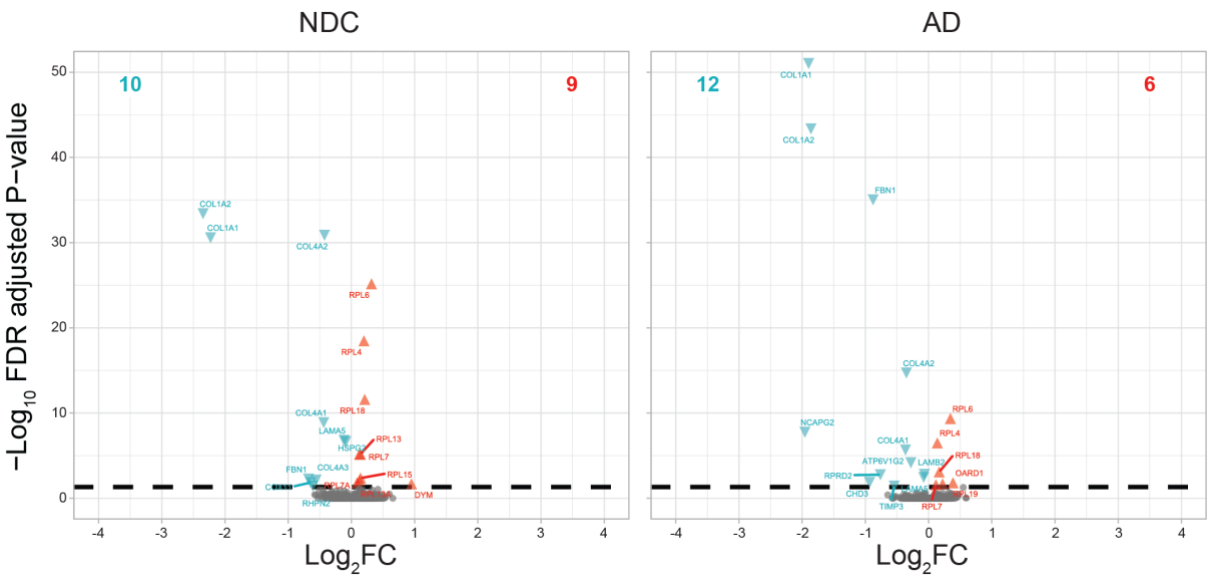


***Figure 2. Protein (de-)enrichment by centrifugation of samples.*** *Volcano plots showing the MSqRob contrast of pre- vs. post-centrifugation samples at 95 °C, for control samples (NDC, left) and AD samples (AD, right). Gene symbols are shown for the top 25 proteins with lowest adjusted p-value that are centrifugation-depleted (turquoise) or centrifugation-enriched (red). The total number of differentially expressed proteins (all above dashed black line) is indicated at the top (left, turquoise; right, red). Overall, the difference in protein abundance due to centrifugation is minimal, and greatly similar between the NDC and AD samples. For a complete list of proteins, see Supplemental file 1.*

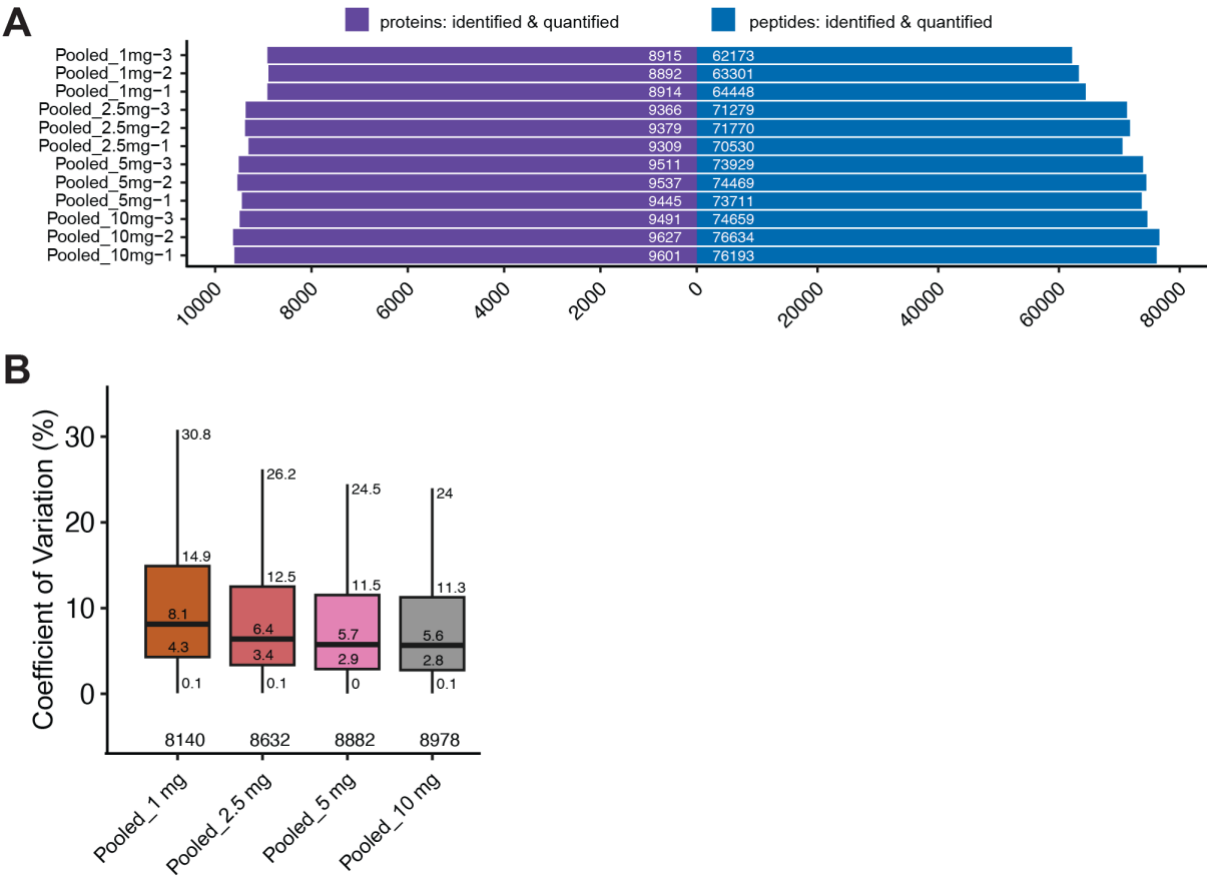


***Figure 3. Quality controls for trypsin digestion efficiency****. A) Protein and peptide counts of samples simulating 1.0, 2.5, 5.0, and 10.0 mg tissue weight input, measured in triplicate (1-2-3), after digestion with 1 µg trypsin (ratio of enzyme : protein = 1:5, 1:12.5, 1:25, 1:50, respectively, with 1:20 being the optimal ratio). Number of detected peptides and proteins increased with increasing simulated input weight. B) Protein-level coefficient of variation of all sample conditions. Values of quartiles and whiskers, and total number of proteins are indicated.*

protein aggregates that might arise using different tissue input.

The final step in optimizing the protocol involved testing whether the calculated amount of trypsin was indeed optimal for effective digestion of our samples. For this, samples from the previous experiments were pooled and diluted to simulate inputs equivalent to 1.0, 2.5, 5.0, and 10.0 mg tissue weight, reflecting the variability of our sample weight. The trypsin amountchosen (1 µg) worked optimally for simulated weight input ≥ 5 mg, showing an increased peptide and protein count and a reduced coefficient of variation (Figure 3A, B). Thus, we strived for sample input being in the range of 5.0–10.0 mg for our subsequent experiments.

Based on the results of our pilot experiments, we established the following optimized protocol: 1) Using samples of 5–10 mg tissue weight, protein solubilization was performed in 500 µL 5% SDS buffer at 95 °C for 15 minutes, with a 15-minute cool-down to 55 °C to avoid safe-lock tubes from opening due to pressure build-up. 2) Extracted proteins were centrifuged to ensure a more representative sample by removing potential aggregates. 3) Trypsin digestion was carried out using a fixed trypsin-to-estimated protein ratio of 1:25 for samples

derived from tissue weight 5–10 mg (whenever available). For each of the specific steps, see supplemental protocol 1.

***2. Subcellular Fraction Isolation: Synaptosome Proteomics***

Proteomic technologies have advanced rapidly, particularly in terms of sensitivity and quantification of proteins relative to the input material required. Subcellular fractionation –such as synaptosome isolation in neuroscience studies [21]– has been commonly employed to reduce sample complexity and enrich for relevant protein subsets [22], thereby overcoming limitations in detection and quantification. However, with current mass-spectrometers now capable of identifying ~10,000 proteins, such detection limits have become less of a bottleneck. In this context, we evaluated whether isolating synaptosome fractions would still provide an advantage in detecting low-abundant synaptic proteins compared to whole-tissue lysates. To test this, we performed a quantitative proteomics analysis comparing whole-tissue lysates and synaptosome-enriched lysates from the same set of NDC donors within the NBB-cohort (n=8; 4 females, see Table 1). We collected 5.0 mg GM (10 µm sections) for whole-tissue analysis and 25.0 mg GM (50 µm sections). Synaptosomes were isolated using an in-house subcellular fractionation protocol (Supplemental protocol 2). The S-TRAP solubilization process was adapted slightly to accommodate the distinct nature of the synaptosome samples but was otherwise followed as previously described (Supplemental protocol 1). All samples were randomized to avoid batch effects.

Although the experiment was originally designed for a paired analysis of whole-tissue vs. synaptosome samples from the same donor, one whole-tissue lysate sample failed to meet the quality control criteria. Furthermore, the paired analysis (n = 7; data not shown) yielded results comparable to those obtained using a standard MS-DAP analysis with the MSqRob model, suggesting that pairing offered limited additional insight, most likely due to inherent biological differences between synaptosome and whole-tissue samples. Therefore, we proceeded with an unpaired MSqRob analysis using age and sex as covariates, comparing whole-tissue and synaptosome groups directly. Using a relatively stringent detection limit (2 peptides, 75% detection per group), we confidently measured 6402 proteins in both whole-tissue lysate and synaptosome preparations (Figure 4A; Supplemental file 2), of which 1302 proteins were annotated as synaptic using the synaptic gene ontology online tool SynGO (SynGO release 1.2, [17]). Note that when using DIA for quantification, peptides need to be detected across samples. For some proteins that were confidently detected in the lysate sample, no peptides were detected after synaptosome isolation (truly “lost” proteins; Supplemental file 2). These were only a small fraction of the total amount (317/(317+6402) = 4.72%), of which 10 were annotated as synaptic in SynGO. These proteins belonged to the nucleus (Supplemental Figure S5), as could be expected from the way synaptosomes are isolated (See Supplemental Protocol 2). From the entire SynGO database, 318 proteins were not detected in either sample. Together with the 10 lysate-specific proteins, these were labeled as ‘absent’ proteins (cf. Figure 4A) and mainly belonged to acetylcholine receptor subunits, as well as receptor proteins from several families (Supplemental Figure S5, Supplemental file 2).

Comparative LC-MS/MS analysis between whole-tissue lysate vs. synaptosome showed the

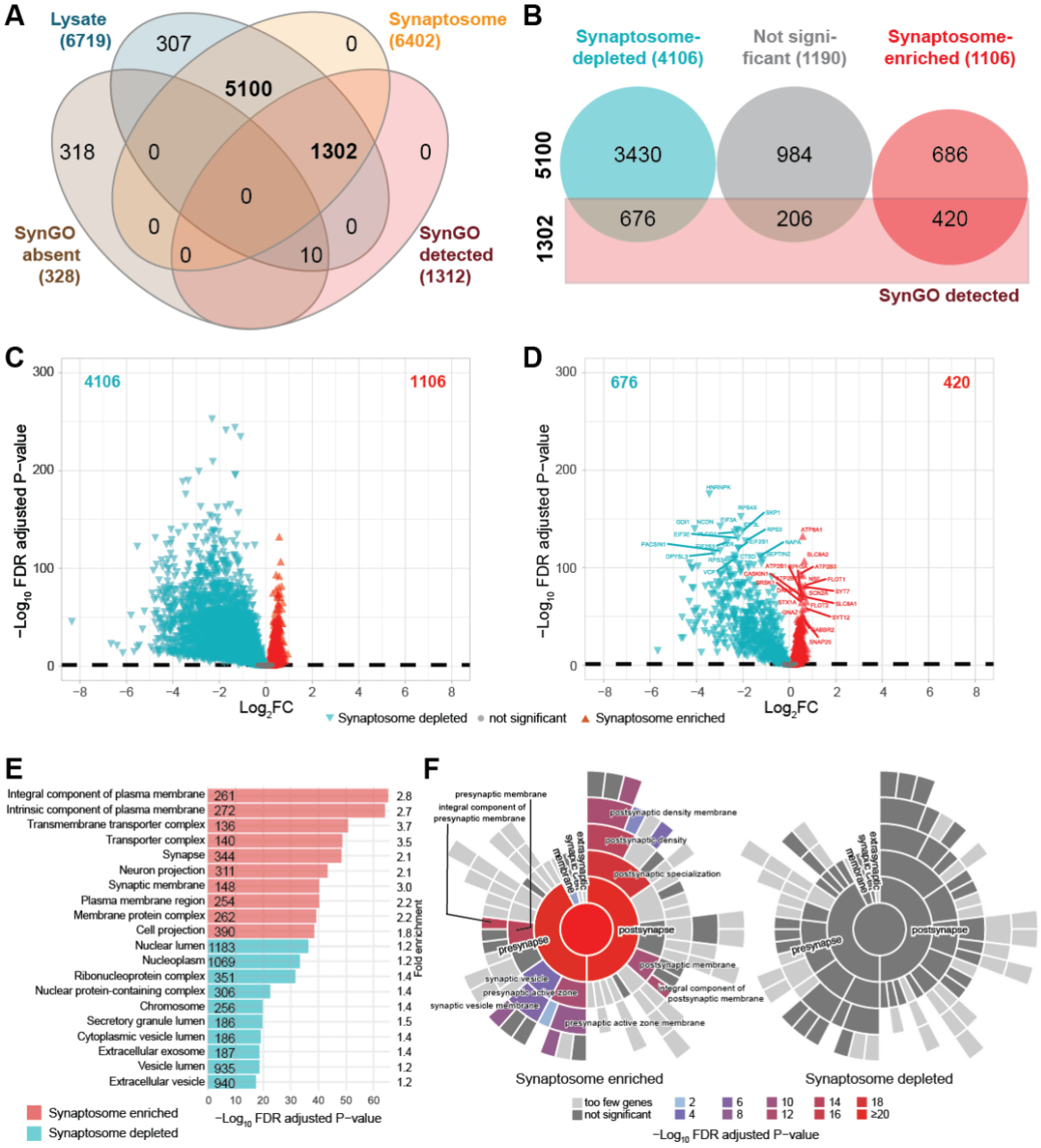


***Figure 4.*** *Enrichment of synaptic proteins in the synaptosome fraction. A) Venn diagram showing the total number of detected proteins and the proportion of SynGO annotated synaptic proteins ("SynGO detected") and SynGO proteins not detected in whole-tissue lysate ("Lysate") and synaptosome ("Synaptosome") samples. B) Diagram showing the division of proteins of the contrast of whole-tissue lysate vs. synaptosome samples (Synaptosome depleted, turquoise; synaptosome enriched, red; Not significant, gray; see panel C), and whether or not the proteins were annotated in SynGO (1302 and 5100 resp. in panel A). C) Volcano plot showing the contrast between whole-tissue and synaptosome for NDC donors (n = 7 for whole-tissue vs. n = 8 for synaptosomes). The largest group of proteins shows depletion (turquoise) in the synaptosome samples, while a smaller number of proteins is enriched (red). The total number of differentially expressed proteins (all above dashed black line) is indicated at the top (left, turquoise; right, red). D) Volcano plot of the same contrast as C) but showing only the proteins annotated in SynGO. The top 20 proteins on each side are labelled. E) Bar graph showing the top 10*

*overrepresented GO annotations of synaptosome enriched and depleted proteins using ShinyGO. The number of proteins participating in each pathway, as well as the fold enrichment is indicated. F) Sunburst plots showing the overrepresentation of synaptosome enriched and depleted proteins for cellular component in SynGO. For a complete list of proteins, see Supplemental file 2.*

significant (adjusted P-value <0.05) enrichment of a relative small set of proteins in synaptosomes (1106 out of 6402 = 17.3%), and a marked depletion of a relative large set of proteins (4106 out of 6402 = 64.1%) (Figure 4B,C), of which 38.0% (420 out of 1106) and 16.5% (676 out of 4106) were annotated as synaptic proteins, respectively. Specifically focusing on the 1302 (420+676+206 non-regulated) detected SynGO proteins in this contrast showed enrichment of typical synaptic proteins, such as proteins of the SNARE (Soluble NSF Attachment Receptor) complex STX1A and SNAP25 [23], and the metabotropic $GABA_B$ receptor subunit B2 [24] (Figure 4D). Gene-set enrichment using the gene ontology tool ShinyGO [18] showed that proteins enriched in synaptosomes were predominantly associated with membrane components and synaptic compartments (Figure 4E). In contrast, proteins enriched in whole-tissue lysates (i.e., synaptosome-depleted) were overrepresented in categories such as nucleus, cytoplasm, extracellular vesicles, chromatin, and ribonucleoprotein complexes (Figure 4E). A more in-depth examination of synapse-specific proteins using SynGO showed a significant overrepresentation in both presynaptic and postsynaptic compartments for the 420 synaptosome enriched SynGO proteins (Figure 4D). Although many SynGO proteins were detected in the synaptosome depleted set, these 676 proteins did not show significant enrichment for cellular localization terms (Figure 4F).

Previous correlation profiling of subcellular fractions from mouse hippocampus, cortex, and cerebellum—including microsomes, synaptosomes, synaptic membranes, and postsynaptic densities—revealed consistent patterns of functional grouping and subcellular localization [8]. Based on these findings, we selected a set of mouse proteins that were previously identified as either enriched (n = 79) or depleted (n = 117) in synaptosomes and synaptic membranes from the cortex. Of these, we detected 77 synapse-enriched and 100 synapse-depleted orthologs in our human cortex proteomics dataset. Notably, the majority of these proteins exhibited similar relative abundance patterns in the human samples, with a strong and statistically significant correlation between mouse and human data (Pearson r = 0.69, P < 0.001; Figure 5A). Among the human proteins that mirrored the synaptic enrichment or depletion observed in mice (49 and 95 proteins, respectively), functional annotation revealed localization to either pre- and post-synaptic compartments or to cytosolic, vesicular, or membrane-associated structures (Figure 5B,C). Three notable subsets among the synapse-depleted proteins were the relatively high enrichment of the postsynaptic (intermediate filament) cytoskeleton and neurofilament groups, which included proteins like neurofilament medium chain (NEFM), neurofilament light chain (NEFL), and alpha-internexin (INA) (see Supplemental file 2). All three are known to function in the postsynaptic compartment [25,26], and are indeed enriched in the postsynaptic density fraction, but not in the synapse fractions [8]. We found all three cytoskeletal proteins consistently identified with high confidence, each supported by more than 50 unique peptides, and they were equally detected across both

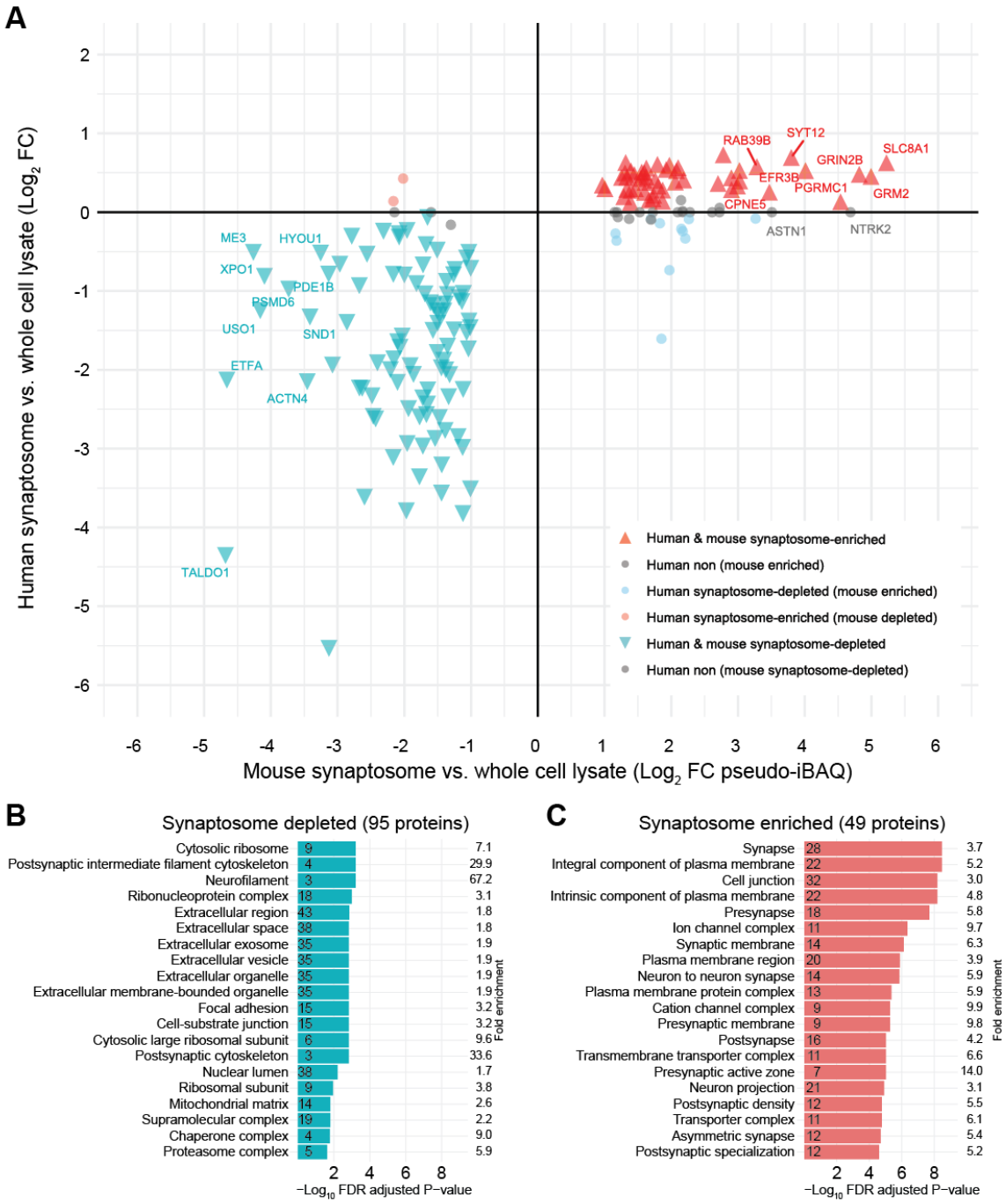


***Figure 5. Cross-validation of synaptosome enrichment and depletion.*** *A) Using a previously published dataset of mouse cortical synapse-enriched and depleted proteins by differential biochemical fractionation [8], selected proteins (n=177) were retrieved from our human NDC lysate vs. synaptosome data set and their relative ratios (log2) were compared. The top 10 proteins with the highest enrichment in mouse synapses are labeled. B,C) Bar graph showing the top 20 overrepresented GO annotations of mouse synaptosome (pseudo-iBAQ values) and human synaptosome proteins that were both synaptosome depleted (B) and enriched (C) using ShinyGO. The number of proteins participating in each annotation, as well as the fold enrichment is indicated. For a complete list of proteins in each analysis, see Supplemental file 2.*

sample types. Hence, the observed synaptosome-depletion stems from differences in relative abundance and subcellular localization (post-synaptic density-enriched) rather than technical variability.

## Discussion & Conclusion

In this study, we optimized our existing protocols to prepare and process human GM samples from post-mortem frozen brain tissue to perform neuroproteomic analyses with LC-MS/MS in the most efficient manner. The first consideration was the type of tissue solubilization as it is a critical preparatory step in proteomic workflows, and directly influences protein yield, integrity, and the breadth of proteome coverage. Two principal strategies are commonly employed: mechanical and chemical solubilization. Mechanical disruption methods—such as tissue grinding, bead beating, and sonication—are widely used to break down the structural integrity of tissues and cellular membranes. These approaches are particularly valuable for subcellular proteomics applications, such as the isolation of organelles or synaptic compartments [27,28]. However, mechanical methods can introduce batch-to-batch variability and are sensitive to technical inconsistencies, particularly when sample sizes are small or heterogeneous. In contrast, chemical solubilization relies on the use of surfactants (e.g., SDS, Triton X-100, CHAPS) and chaotropic agents (e.g., urea, thiourea, guanidine hydrochloride) to denature and solubilize proteins, including membrane-associated and hydrophobic proteins that are typically underrepresented in proteomic analyses [29]. The use of well-defined buffer compositions improves reproducibility and facilitates scalability, making chemical lysis particularly well suited for high-throughput proteomic pipelines. A limitation of this approach is the need to remove interfering reagents prior to LC-MS/MS analysis, which can be effectively achieved through protein precipitation or filter-based methods such as the S-TRAP protocol [12].

Post-mortem brain samples are often received as frozen tissue blocks and may be processed for multiple downstream applications, including proteomics and immunohistochemistry. In this context, the separation of GM from white matter (WM) provides a critical advantage. GM is enriched in neuronal cell bodies and synaptic components, while WM contains abundant myelin proteins and oligodendrocyte-derived material. Analyzing GM separately improves the detection of lower-abundance synaptic proteins that could otherwise be masked by highly abundant myelin proteins, thereby increasing the biological specificity and interpretability of proteomic data. For this reason, we optimized the pre-MS protocol for whole-tissue lysate using thin (10 µm) GM sections.

First, we optimized the ProtiFi S-TRAP mini spin column digestion protocol 4.1 for LC-MS/MS proteomics to accommodate the specific requirements of our sample size and tissue quantity. To ensure complete solubilization of 10 µm-thick tissue sections, we increased the temperature during the solubilization step. We retained a final centrifugation step in the protocol to maximize recovery and ensure representative sample collection. Additionally, we standardized the ratio of trypsin-to-protein. Together, these tests and protocol adaptations ensured a highly standardized and efficient sample preparation workflow—crucial when expecting subtle biological effects. An important consideration throughout the entire experimental process –including tissue dissection and LC-MS/MS analysis– is a strict

standardization and randomization. This is especially important in large-scale studies where experiments are spread out over days or even months. To mitigate confounding batch effects in the interpretation of the resulting data, we distributed the samples of each experimental group evenly across experimental batches for every experimental step, and all procedures were performed in a consistent manner. The sequence of sample dissection, S-TRAP preparation, and LC-MS/MS analysis was carefully arranged and randomized to avoid confounding effects. Notably, we observed a trend in LC-MS/MS analysis where the order of samples run affected the number of identified peptides (see Supplemental Figure S1). This underscores the critical role of rigorous standardization and randomization in large-scale proteomic workflows to ensure that technical variation affects all experimental groups equally. The procedures described here may serve as a practical guide for researchers aiming to standardize and refine neuroproteomics, from human brain tissue dissection through LC-MS/MS analysis.

Secondly, we compared whole-tissue and synaptosome proteomics to assess their relative strengths in detecting disease-relevant protein changes and observed that MS sensitivity is sufficient to detect most of the low-abundant (synaptic) proteins across the tissue measured. As such, we propose to first execute a whole-tissue analysis to detect disease-induced proteomic changes. This approach offers a broad, rapid and relatively easily executed overview of molecular changes without compromising the detection of low-abundance synaptic proteins. Whole-tissue analysis is particularly advantageous when tissue is collected in parallel for both whole-tissue and synaptosome preparations as we described here. In such cases, initial whole-tissue data can highlight key biological processes or pathways that may warrant deeper, targeted investigation. Moreover, synaptosome preparation is inherently more time-consuming, labor-intensive, and hence leads to a higher between-sample variability, which may limit its practicality in large-scale studies.

Although the coverage of synaptic proteins in whole-tissue proteomics was similar to that of synaptosome-enriched samples (see Figure 4), subtle or compartment-specific protein regulation at the synapse could be missed in whole-tissue datasets—considering that most synaptic proteins are also expressed in non-synaptic compartments. In such cases, synaptosome isolation could provide added value by enriching for synaptic proteins, thereby reducing interference from non-synaptic proteins and offering a clearer view of synapse-specific regulation. However, an important caveat in synaptosome proteomics is normalization of protein levels across samples, which can obscure protein-level differences driven by changes in synapse number—particularly relevant in conditions where synapse loss or gain is suspected [4,30], as evidenced by prior proteomic or immunohistochemical data.

Therefore, we recommend a tiered strategy: initiate analysis with whole-tissue proteomics to identify disease-associated processes and follow up with synaptosome proteomics on pre-dissected samples to gain deeper insight into synaptic composition and population-level changes. This combined approach maximizes sensitivity, specificity, and interpretability across both cellular and subcellular levels.

## Supplementary Materials & data availability

The following supporting information is available:

- Figure S1: Necessity of randomization in MS work-flow;
- Figure S2: Determining isolated protein amount by BCA test;
- Figure S3: Number of peptides/proteins detected in pilot;
- Figure S4: (De)enrichment of proteins by centrifugation is minimal;
- Figure S5: Protein pathways of lost synaptosome proteins and absent SynGO proteins;
- Supplementary File 1: Differential abundance protocol optimization, contains quantification results for the pilot proteomics experiment (relates to Figures 1–3), testing temperature, centrifugation and trypsin concentration on NDC and AD samples;
- Supplementary File 2: NDC Lysate vs. Synaptosomes, contains quantification results for the whole cell lysate vs synaptosome proteomics experiment (relates to Figures 4 & 5), on NDC samples;
- Supplementary protocol 1: S-TRAP pre-MS proteomics, contains the step-by-step optimized pre-MS protocol for whole cell lysate samples (tissue sections cut at 10 µm);
- Supplementary protocol 2: Synaptosome isolation, contains the step-by-step optimized protocol for synaptosome isolation from 50 µm tissue sections.

## Author Contribution

Conceptualization, FRK, RVK, and SS; Methodology, FRK, RVK, TSZK; Validation, FRK, RVK, ABS and FTWK; Formal Analysis, FRK, RVK and FTWK; Investigation, FRK; Data Curation, SS; Visualization, FRK, ABS and SS; Writing – Original Draft Preparation, FRK, TSZK and SS; Writing – Review & Editing, FRK, FTWK, RVK, TSZK, ABS and SS; Supervision, ABS and SS; Funding Acquisition, FRK and SS. All authors have read and agreed to the published version of the manuscript.

## Funding

FRK and SS were supported by an NWO VICI grant (ALW-Vici 016.150.673 / 865.14.002); FRK was supported by Proof-of-Concept funding from Amsterdam Neuroscience, Amsterdam.

## Informed Consent & ethical approval

Tissue was obtained from the Netherlands Brain Bank (NBB). Informed consent was obtained from all donors for the use of material and clinical data for research purposes. The NBB autopsy procedures and the use of tissue for research were approved by the Ethics Committee of Amsterdam UMC, location VUmc, Amsterdam, The Netherlands.

## Acknowledgments

This work would not have been possible without the help of Berna Özer, who assisted in sample preparation across experiments. Brain tissue was made available by Inge Huitinga, head of the Neuroimmunology group at the Netherlands Institute for Neuroscience, Amsterdam. We would also like to thank Dennis Wever (Huitinga group), his expertise in the free-hand dissection of GM was essential for the tissue collection. During the preparation of this manuscript, the authors used ChatGPT (OpenAI, GPT-4) for the purpose of text editing. The authors have reviewed and edited the output and take full responsibility for the content of this publication.

## Conflicts of Interest:

The authors declare no conflicts of interest.

## Abbreviations

The following abbreviations are used in this manuscript:

| | |
|---|---|
| LC-MS/MS | Liquid Chromatography-tandem Mass Spectrometry |
| S-TRAP | Suspension-TRAPping |
| NBB | Netherlands Brain Bank |
| SFG | Superior Frontal Gyrus |
| NDC | Non-Demented Control |
| AD | Alzheimer's Disease |
| GM | Gray Matter |
| PMI | Post-Mortem Interval |
| Braak LB | Braak Lewy Bodies |
| APOE | Apolipoprotein E |
| SDS | Sodium Dodecyl Sulfate |
| BCA | Bicinhoninic Acid |
| MSqRob | Robust statistical inference for quantitative LC-MS proteomics |
| DIA-NN | Data-Independent Acquisition - Neural Networks |
| dia-PASEF | Data-Independent Acquisition - Parallel Accumulation Serial Fragmentation |
| VSN | Variable Sorting for Normalization |
| MS-DAP | Mass Spectrometry Downstream Analysis Pipeline |
| FDR | False Detection Rate |
| SynGO | Synaptic Gene Ontology |
| ShinyGO | Shiny Gene Ontology |
| DIA | Data-Independent Acquistion |
| SNARE | Soluble NSF Attachment Receptor |
| GO | Gene Ontology |
| CHAPS | 3-[(3-cholamidopropyl)dimethylammonio]-1-propanesulfonate |
| WM | White Matter |

## References


1. Huitinga, I. *Handbook of Clinical Neurology*; Huitinga, I., Webster, M.J., Eds.; 1st Edition.; Elsevier, 2018; Vol. Volume 150: Brain Banking; ISBN 9780444636423.

2. Piehowski, P.D.; Petyuk, V.A.; Orton, D.J.; Xie, F.; Moore, R.J.; Ramirez-Restrepo, M.; Engel, A.; Lieberman, A.P.; Albin, R.L.; Camp, D.G.; et al. Sources of Technical Variability in Quantitative LC–MS Proteomics: Human Brain Tissue Sample Analysis. *J. Proteome Res.* **2013**, *12*, 2128–2137, doi:10.1021/pr301146m.

3. Nachman, E.; Verstreken, P. Synaptic Proteostasis in Parkinson's Disease. *Curr. Opin. Neurobiol.* **2022**, *72*, 72–79, doi:10.1016/j.conb.2021.09.001.

4. Griffiths, J.; Grant, S.G.N. Synapse Pathology in Alzheimer's Disease. *Semin. Cell Dev. Biol.* **2023**, *139*, 13–23, doi:10.1016/j.semcdb.2022.05.028.

5. Mullins, N.; Forstner, A.J.; O'Connell, K.S.; Coombes, B.; Coleman, J.R.I.; Qiao, Z.; Als, T.D.; Bigdeli, T.B.; Børte, S.; Bryois, J.; et al. Genome-Wide Association Study of More than 40,000 Bipolar Disorder Cases Provides New Insights into the Underlying Biology. *Nat. Genet.* **2021**, *53*, 817–829, doi:10.1038/s41588-021-00857-4.

6. Das, S.C.; Hjelm, B.E.; Rollins, B.L.; Sequeira, A.; Morgan, L.; Omidsalar, A.A.; Schatzberg, A.F.; Barchas, J.D.; Lee, F.S.; Myers, R.M.; et al. Mitochondria DNA Copy Number, Mitochondria DNA Total Somatic Deletions, Complex I Activity, Synapse Number, and Synaptic Mitochondria Number Are Altered in Schizophrenia and Bipolar Disorder. *Transl. Psychiatry* **2022**, *12*, 353, doi:10.1038/s41398-022-02127-1.

7. Fries, G.R.; Saldana, V.A.; Finnstein, J.; Rein, T. Molecular Pathways of Major Depressive Disorder Converge on the Synapse. *Mol. Psychiatry* **2023**, *28*, 284–297, doi:10.1038/s41380-022-01806-1.

8. Pandya, N.J.; Koopmans, F.; Slotman, J.A.; Paliukhovich, I.; Houtsmuller, A.B.; Smit, A.B.; Li, K.W. Correlation Profiling of Brain Sub-Cellular Proteomes Reveals Co-Assembly of Synaptic Proteins and Subcellular Distribution. *Sci. Rep.* **2017**, *7*, 12107, doi:10.1038/s41598-017-11690-3.

9. Wang, H.; Dey, K.K.; Chen, P.-C.; Li, Y.; Niu, M.; Cho, J.-H.; Wang, X.; Bai, B.; Jiao, Y.; Chepyala, S.R.; et al. Integrated Analysis of Ultra-Deep Proteomes in Cortex, Cerebrospinal Fluid and Serum Reveals a Mitochondrial Signature in Alzheimer's Disease. *Mol. Neurodegener.* **2020**, *15*, 43, doi:10.1186/s13024-020-00384-6.

10. Johnson, E.C.B.; Dammer, E.B.; Duong, D.M.; Ping, L.; Zhou, M.; Yin, L.; Higginbotham, L.A.; Guajardo, A.; White, B.; Troncoso, J.C.; et al. Large-Scale Proteomic Analysis of Alzheimer's Disease Brain and Cerebrospinal Fluid Reveals Early Changes in Energy Metabolism Associated with Microglia and Astrocyte Activation. *Nat. Med.* **2020**, *26*, 769–780, doi:10.1038/s41591-020-0815-6.

11. Seifar, F.; Fox, E.J.; Shantaraman, A.; Liu, Y.; Dammer, E.B.; Modeste, E.; Duong, D.M.; Yin, L.; Trautwig, A.N.; Guo, Q.; et al. Large-scale Deep Proteomic Analysis in Alzheimer's Disease Brain Regions across Race and Ethnicity. *Alzheimer's Dement.* **2024**, *20*, 8878–8897, doi:10.1002/alz.14360.

12. Thanou, E.; Koopmans, F.; Pita-Illobre, D.; Klaassen, R.V.; Özer, B.; Charalampopoulos, I.; Smit, A.B.; Li, K.W. Suspension TRAPping Filter (STRAP) Sample Preparation for

Quantitative Proteomics in the Low Mg Input Range Using a Plasmid DNA Micro-Spin Column: Analysis of the Hippocampus from the 5xFAD Alzheimer's Disease Mouse Model. *Cells* **2023**, *12*, 1242, doi:10.3390/cells12091242.

13. Ding, S.; Royall, J.J.; Sunkin, S.M.; Ng, L.; Facer, B.A.C.; Lesnar, P.; Guillozet-Bongaarts, A.; McMurray, B.; Szafer, A.; Dolbeare, T.A.; et al. Comprehensive Cellular-resolution Atlas of the Adult Human Brain. *J. Comp. Neurol.* **2016**, *524*, 3127–3481, doi:10.1002/cne.24080.

14. Skowronek, P.; Thielert, M.; Voytik, E.; Tanzer, M.C.; Hansen, F.M.; Willems, S.; Karayel, O.; Brunner, A.-D.; Meier, F.; Mann, M. Rapid and In-Depth Coverage of the (Phospho-)Proteome With Deep Libraries and Optimal Window Design for Dia-PASEF. *Mol. Cell. Proteom.* **2022**, *21*, 100279, doi:10.1016/j.mcpro.2022.100279.

15. Demichev, V.; Messner, C.B.; Vernardis, S.I.; Lilley, K.S.; Ralser, M. DIA-NN: Neural Networks and Interference Correction Enable Deep Proteome Coverage in High Throughput. *Nat. Methods* **2020**, *17*, 41–44, doi:10.1038/s41592-019-0638-x.

16. Koopmans, F.; Li, K.W.; Klaassen, R.V.; Smit, A.B. MS-DAP Platform for Downstream Data Analysis of Label-Free Proteomics Uncovers Optimal Workflows in Benchmark Data Sets and Increased Sensitivity in Analysis of Alzheimer's Biomarker Data. *J. Proteome Res.* **2023**, *22*, 374–386, doi:10.1021/acs.jproteome.2c00513.

17. Koopmans, F.; Nierop, P. van; Andres-Alonso, M.; Byrnes, A.; Cijsouw, T.; Coba, M.P.; Cornelisse, L.N.; Farrell, R.J.; Goldschmidt, H.L.; Howrigan, D.P.; et al. SynGO: An Evidence-Based, Expert-Curated Knowledge Base for the Synapse. *Neuron* **2019**, *103*, 217-234.e4, doi:10.1016/j.neuron.2019.05.002.

18. Ge, S.X.; Jung, D.; Yao, R. ShinyGO: A Graphical Gene-Set Enrichment Tool for Animals and Plants. *Bioinformatics* **2019**, *36*, 2628–2629, doi:10.1093/bioinformatics/btz931.

19. Heberle, H.; Meirelles, G.V.; Silva, F.R. da; Telles, G.P.; Minghim, R. InteractiVenn: A Web-Based Tool for the Analysis of Sets through Venn Diagrams. *BMC Bioinform.* **2015**, *16*, 169, doi:10.1186/s12859-015-0611-3.

20. Laskowska, E.; Kuczyńska-Wiśnik, D.; Lipińska, B. Proteomic Analysis of Protein Homeostasis and Aggregation. *J. Proteom.* **2019**, *198*, 98–112, doi:10.1016/j.jprot.2018.12.003.

21. Tieze, S.M.; Chandra, S.S.; Vidyadhara, D.J. Subcellular Fractionation for the Isolation of Synaptic Components from the Murine Brain. *J. Vis. Exp.* **2022**, doi:10.3791/64574.

22. Kislinger, T.; Cox, B.; Kannan, A.; Chung, C.; Hu, P.; Ignatchenko, A.; Scott, M.S.; Gramolini, A.O.; Morris, Q.; Hallett, M.T.; et al. Global Survey of Organ and Organelle Protein Expression in Mouse: Combined Proteomic and Transcriptomic Profiling. *Cell* **2006**, *125*, 173–186, doi:10.1016/j.cell.2006.01.044.

23. Hanson, P.I.; Roth, R.; Morisaki, H.; Jahn, R.; Heuser, J.E. Structure and Conformational Changes in NSF and Its Membrane Receptor Complexes Visualized by Quick-Freeze/Deep-Etch Electron Microscopy. *Cell* **1997**, *90*, 523–535, doi:10.1016/s0092-8674(00)80512-7.

24. Kulik, A.; Vida, I.; Luján, R.; Haas, C.A.; López-Bendito, G.; Shigemoto, R.; Frotscher, M. Subcellular Localization of Metabotropic GABAB Receptor Subunits GABAB1a/b and

GABAB2 in the Rat Hippocampus. *J. Neurosci.* **2003**, *23*, 11026–11035, doi:10.1523/jneurosci.23-35-11026.2003.

25. Suzuki, T.; Mitake, S.; Okumura-Noji, K.; Shimizu, H.; Tada, T.; Fujii, T. Excitable Membranes and Synaptic Transmission: Postsynaptic Mechanisms. Localization of α-Internexin in the Postsynaptic Density of the Rat Brain. *Brain Res.* **1997**, *765*, 74–80, doi:10.1016/s0006-8993(97)00492-7.

26. Yuan, A.; Nixon, R.A. Specialized Roles of Neurofilament Proteins in Synapses: Relevance to Neuropsychiatric Disorders. *Brain Res. Bull.* **2016**, *126*, 334–346, doi:10.1016/j.brainresbull.2016.09.002.

27. Gulyássy, P.; Puska, G.; Györffy, B.A.; Todorov-Völgyi, K.; Juhász, G.; Drahos, L.; Kékesi, K.A. Proteomic Comparison of Different Synaptosome Preparation Procedures. *Amino Acids* **2020**, *52*, 1529–1543, doi:10.1007/s00726-020-02912-6.

28. Riga, D.; Kramvis, I.; Koskinen, M.K.; Bokhoven, P. van; Harst, J.E. van der; Heistek, T.S.; Timmerman, A.J.; Nierop, P. van; Schors, R.C. van der; Pieneman, A.W.; et al. Hippocampal Extracellular Matrix Alterations Contribute to Cognitive Impairment Associated with a Chronic Depressive-like State in Rats. *Sci. Transl. Med.* **2017**, *9*, doi:10.1126/scitranslmed.aai8753.

29. Masuda, T.; Tomita, M.; Ishihama, Y. Phase Transfer Surfactant-Aided Trypsin Digestion for Membrane Proteome Analysis. *J. Proteome Res.* **2008**, *7*, 731–740, doi:10.1021/pr700658q.

30. Dorostkar, M.M.; Zou, C.; Blazquez-Llorca, L.; Herms, J. Analyzing Dendritic Spine Pathology in Alzheimer's Disease: Problems and Opportunities. *Acta Neuropathol.* **2015**, *130*, 1–19, doi:10.1007/s00401-015-1449-5.

## Supplemental figures:

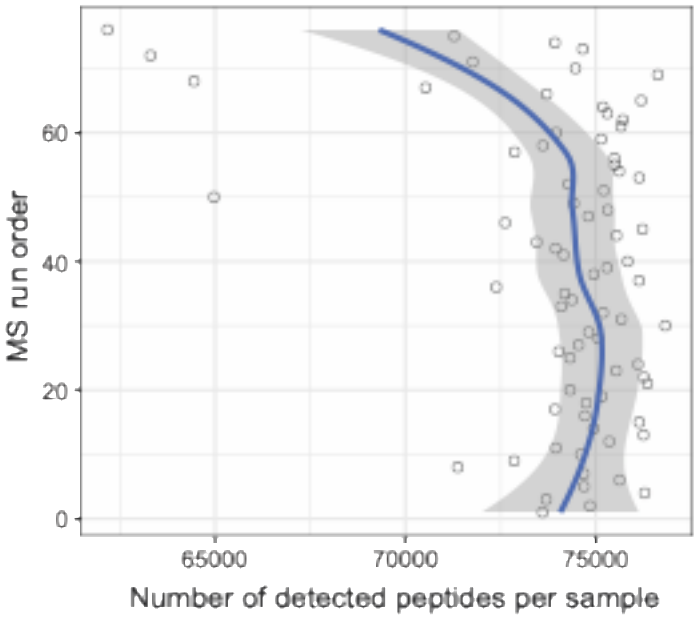


***Figure S1. Necessity of randomization in MS workflow.*** *One of the standard quality controls from the MS-DAP analysis shows the effect of the order in the MS analysis on the number of peptides detected. This emphasizes the importance of randomizing the samples across experimental groups to avoid technical effects biasing the results.*

**A**

| Samples | OD | µg/µL | Total µg in 750 uL |
|---|---|---|---|
| pre AD_A | 0.475 | 1.21 | 906.49 |
| pre AD_B | 0.488 | 1.24 | 931.30 |
| pre NDC_A | 0.477 | 1.21 | 910.31 |
| pre NDC_B | 0.484 | 1.23 | 923.66 |
| post AD_A | 0.481 | 1.22 | 917.94 |
| post AD_B | 0.483 | 1.23 | 921.76 |
| post NDC_A | 0.478 | 1.22 | 912.21 |
| post NDC_B | 0.480 | 1.22 | 916.03 |

**B**

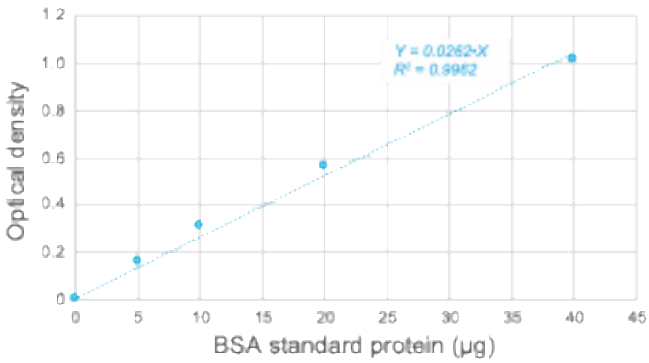


***Figure S2. Determining isolated protein amount by BCA test.*** *Optical density was measured for bovine serum albumin (BSA) standards (left) and was used to extrapolate protein concentration based on the OD of 15 µL from our samples (right). On average, our samples contained around 900 µg protein in 10 mg of initial tissue weight (dissolved in 750 µL 5% SDS for the OD measurements above). No weight loss was encountered by centrifugation. Pre = pre-centrifugation; Post = post-centrifugation; NDC = non-demented control donor; AD = donor with Alzheimer's Disease.*

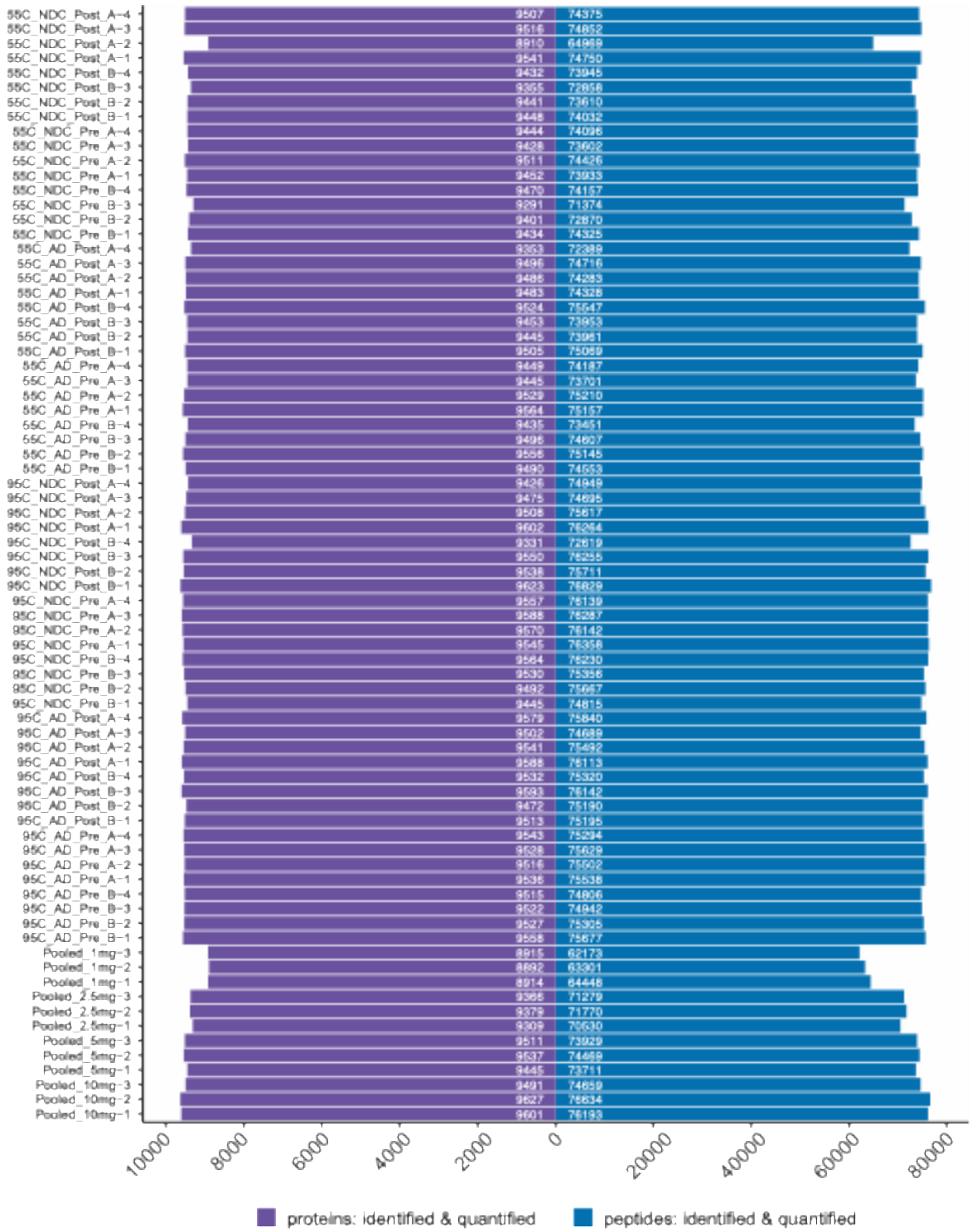


***Figure S3. Number of peptides/proteins detected in pilot.*** *This plot shows the number of (target) peptides that are detected per sample, as well as total protein number. For DIA, we refer to a peptide as 'detected' if the confidence score (for identification) is <= 0.01.*

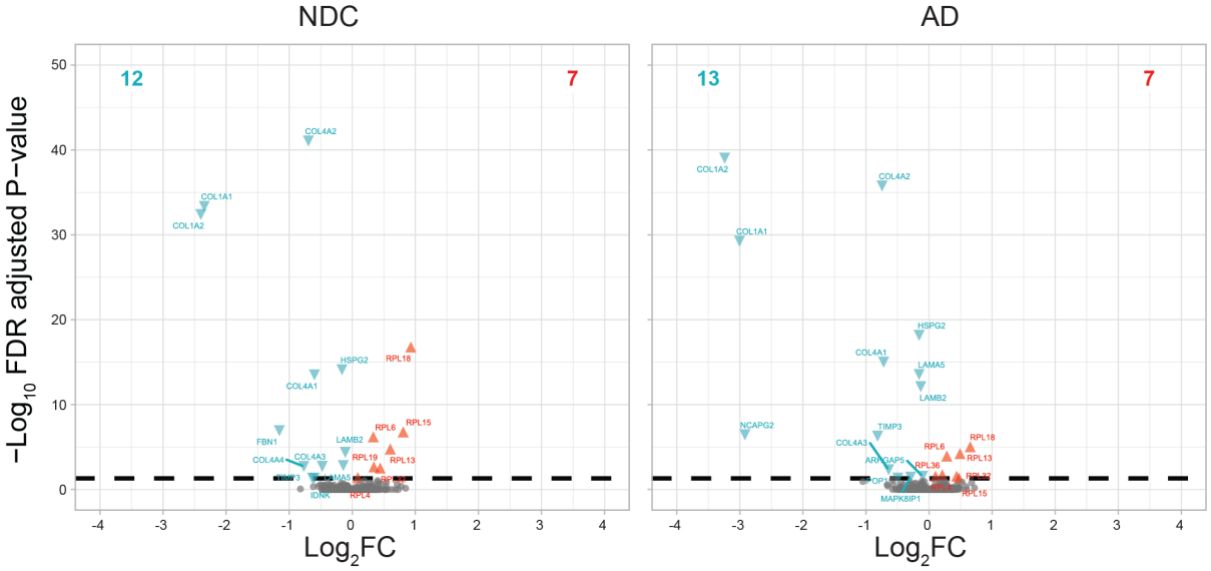


***Figure S4. (De)enrichment of proteins by centrifugation is minimal.*** *Volcano plots showing the MSqRob contrast of pre- vs. post-centrifugation for samples lysed at 55 °C, for control samples (NDC) and AD samples (AD). Proteins that are "downregulated" in blue are proteins that are less abundant after centrifugation, including multiple collagens. Proteins that are "upregulated" (orange) are proteins whose abundance increases after centrifugation, including multiple ribosomal proteins. Overall, the protein abundance decrease due to centrifugation is minimal, and greatly similar between the control and AD samples. The proteins for which no peptides were detected (truly "lost" proteins after centrifugation; not visible in this graph) only were a very small fraction of the total; Supplemental file 1.*

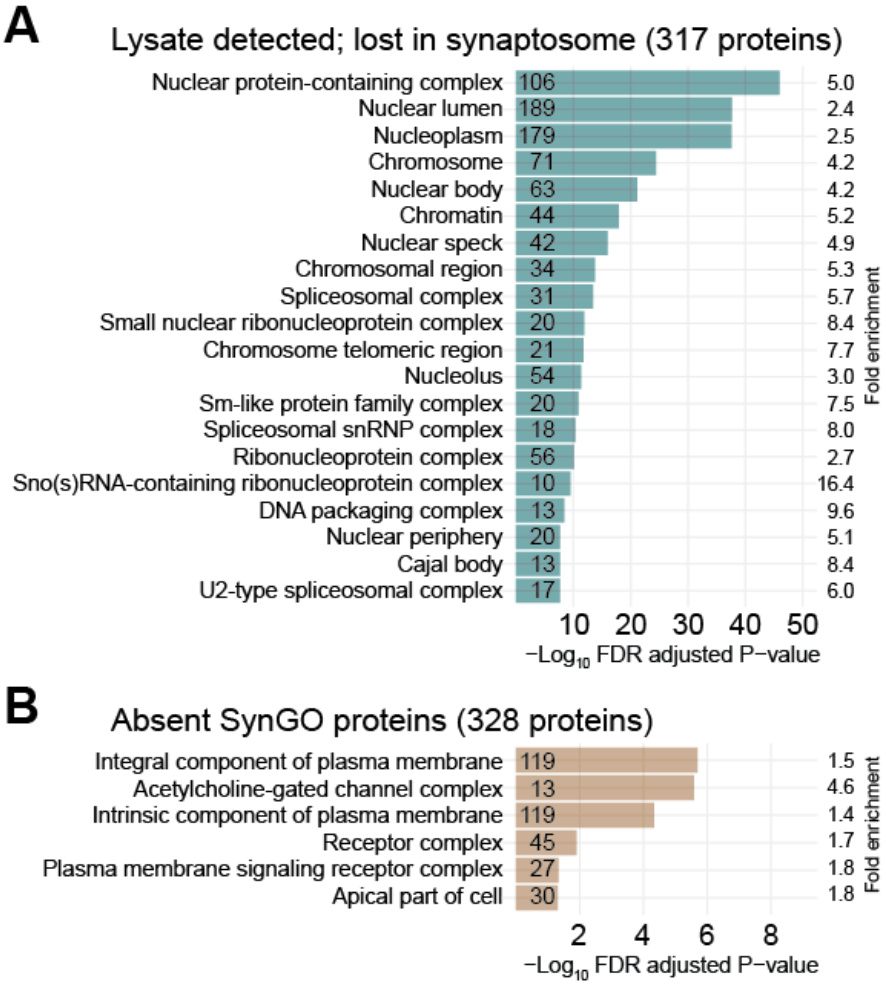


***Figure S5. Protein pathways of lost synaptosome proteins and absent SynGO proteins.*** *A,B) Bar graph showing the top 20 overrepresented GO annotations of the 317 proteins that were not detected in the synaptosome isolation (A), and the 328 SynGO proteins that were not detected in both samples according to the criteria set (B). Note that the x-axis scale for panel A and B is different. For a complete list of proteins in each analysis, see Supplemental file 2.*